Production of multi-strangeness hypernuclei and the YN-interaction

CrossMark

T. Gaitanos [a,*], H. Lenske [a,b]

[a] *Institut für Theoretische Physik, Universität Giessen, D-35392 Giessen, Germany*
[b] *GSI Helmholtzzentrum für Schwerionenforschung, D-64291 Darmstadt, Germany*

A B S T R A C T

We investigate for the first time the influence of hyperon–nucleon (YN) interaction models on the strangeness dynamics of antiproton–nucleus and Ξ–nucleus interactions. Of particular interest is the formation of bound multi-strangeness hypermatter in reactions relevant for $\bar{P}$ANDA. The main features of two well-established microscopic approaches for YN-scattering are first discussed and their results are then analyzed such that they can be applied in transport-theoretical simulations. The transport calculations for reactions induced by antiproton beams on a primary target including also the secondary cascade beams on a secondary target show a strong sensitivity on the underlying YN-interaction. In particular, we predict the formation of Ξ-hypernuclei with an observable sensitivity on the underlying ΞN-interaction. We conclude the importance of our studies for the forthcoming research plans at FAIR.

© 2014 The Authors. Published by Elsevier B.V. This is an open access article under the CC BY license (http://creativecommons.org/licenses/by/3.0/). Funded by SCOAP³.

1. Introduction

A central task of flavor nuclear physics is the construction of a realistic physical picture of nuclear forces between the octet-baryons N, Λ, Σ, Ξ [1–5]. Experimental information on the bare hyperon–nucleon interactions is accessible in the $S = -1$ sector (ΛN and ΣN channels) [6–10], however, empirical data for the $S = -2$ channels involving the cascade hyperon are still very sparse [11]. As a consequence, the parameters of the bare YN-interactions in the $S = -1$ channel are better under control than those parameters in the $S = -2$ sector, e.g., ΞN $\rightarrow$ ΞN, $\Lambda\Lambda$. In fact, various theoretical models, which are based on the well-established one-boson-exchange approach for the NN-interaction or rely on more sophisticated models on the quark level, predict quite different results for the ΞN-channels in vacuum [9, 11]. This is very clearly manifested in the different energy dependence of phase-shifts, which in one model are compatible with an attractive [12], and in another approach with a repulsive [13] ΞN-interactions in free space. Of extreme interest is here the ΞN $\rightarrow$ $\Lambda\Lambda$ channel, because it provides information also on the bare interaction between hyperons themselves and it is the leading channel for the production of double-Λ hypernuclei.

Information of these YN interactions at finite baryon density can be achieved in studies of hypernuclei [14–16] in reactions in-

duced by mesons (π- and K-beams), by high-energy (anti)protons and heavy ions, and by electro-production [18,19]. Recently, the FOPI [20] and HypHI [21] Collaborations at GSI have performed experiments on single-Λ hypernuclei with the analysis being still in progress. The experimental investigation of multi-strangeness, e.g., double-Λ, hypernuclei will be realized in the new FAIR facility at GSI by the $\bar{P}$ANDA Collaboration [22,23]. According to the $\bar{P}$ANDA proposals, multi-strangeness bound hypermatter is supposed to be created in a two-step process through the capture of cascade particles (Ξ) – produced in primary antiproton-induced reactions – on secondary targets. Also theoretical investigations have been started recently [14–17].

We have studied in the past the formation and production mechanisms of hyperons [24], fragments [25] and hyperfragments [14,26] in reactions induced by heavy ions, protons and antiprotons, however, by using fixed interactions for the hyperon–nucleon channels, in particular, in the $S = -2$ sector. The task of the present work is to investigate the role and possible observable effects of different YN-interaction models on the strangeness dynamics of hadron-induced reactions. We have extended our earlier works by considering improved parametrizations for the cross sections of the $S = -2$ YN-channels. They are based on the microscopic calculations of the Nijmegen group by Rijken and Yamamoto [12] and by Fujiwara et al. [13]. In Section 2 we briefly outline the main features of the adopted microscopic YN-calculations and discuss the basic differences between them in terms of scattering observables. For numerical purposes, the

* Corresponding author.
E-mail address: Theodoros.Gaitanos@theo.physik.uni-giessen.de (T. Gaitanos).

theoretical cross sections have been parametrized and implemented into a transport model. We discuss then the transport results of hadron-induced reactions in detail. Our results show strong dynamical effects originating from the different underlying ΞN-interactions. They are clearly visible in the yields of multi-strangeness hypernuclear production in low-energy Ξ-induced reactions. Hence, the proposed production experiments may lead to strong constraints on the high strangeness YN and YY interactions.

2. Hyperon–nucleon interaction models in the $S = -2$ sector

A variety of well-established models concerning the high strangeness sector exists in the literature. Among others, the chiral-unitary approach of Sasaki, Oset and Vacas [10] and the effective field theoretical models of the Bochum/Jülich groups [10] are representative examples. The Nijmegen [12] models are based on the well-known one-boson-exchange formalism to the NN-interaction, which is then extended to the strangeness sector with the help of SU(3) symmetry arguments. Finally, Fujiwara et al. [13] have developed quark-cluster models for the baryon–baryon (BB) interactions in the $S = 0, -1, -2, -3, -4$ sectors.

The parameters are determined by simultaneous fits to NN- and YN-scattering observables in the $S = -1$ sector. While there are several thousand well confirmed experimental data in the $S = 0$ sector (NN scattering), much less data points are safely known for YN reactions. They still allow a reasonable determination of the ΛN and ΣN model parameters. Thus, despite of model differences all the theoretical approaches yield similar predictions for, e.g., potential depths and scattering cross sections for exclusive channels between nucleons and hyperons with strangeness $S = -1$. Remaining uncertainties for $S = -1$ interactions are related to the unsatisfactory experimental data base.

In the $S = -2$ sector, where cascade particles (Ξ) are involved, the uncertainties and, correspondingly, the discrepancies between the models are considerably larger [11]. To demonstrate this issue, we have chosen two particular model calculations to be tested in the present work. The one-boson-exchange calculations of the Nijmegen group in the extended soft-core version ESC04 of 2004 (we call this as ESC in the following) [12] and the quark-cluster approach [13] (denoted as FSS in the following). Note that more modern approaches of the Nijmegen group exist, e.g., the more recent models ESC08 [9]. However, our intention is to investigate possible sensitivities in the dynamics of hadron-induced reactions at P̄ANDA, thus we choose two models which utilize very different physical pictures and exhibit the largest differences in the ΞN-interactions.

Fig. 1 shows the elastic and inelastic scattering cross sections for the isospin $I = 1$ $\Xi N \to \Xi N$ and $\Xi N \to \Lambda\Lambda$ channels, respectively, predicted by the two models as indicated. We show cross sections for the relevant exclusive channels only, as entering into the dynamical calculations (see next section). At first, the ESC calculations predict a stronger energy dependence of the ΞN scattering. This effect is extreme at lower cascade energies, where the inelastic $\Xi N \to \Lambda\Lambda$ channel dominates relative to the elastic one. In fact, this pronounced energy dependence has been observed indirectly in the production of double-strangeness Λ-hypernuclei, where the double-Λ hypernuclei yields dropped considerably with increasing Ξ-beam energy [14]. On the other hand, the FSS calculations predict a much smoother energy behavior of both cross sections, where an opposite trend relative to the ESC results is observed: the $S = -2$ dynamics is largely dominated by the ΞN channel, while the $\Lambda\Lambda$ channel is populated to a lesser degree.

The differences in the cross sections reflect the rather different predictions of the scattering parameters, e.g., the phase shifts for low-energy s-states. The Nijmegen model in the ESC04 version,
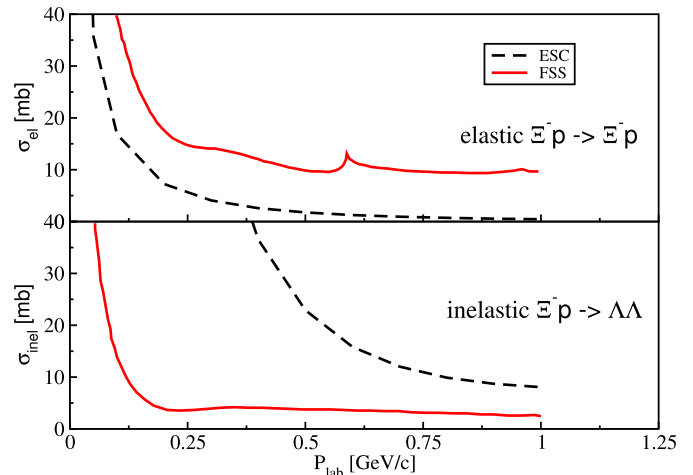

Fig. 1. Elastic (panel on the top) and inelastic (panel on the bottom) cross sections versus the Ξ-beam momentum for the Ξ^-p-channel. Results obtained by the ESC approach (dashed curves [12]) are compared to the FSS model (solid curves [13]).

which is used here, predict negative s-wave phase shifts for the $I = 0$ ΞN channel at various cascade energies indicating a repulsive interaction, while in the $\Lambda\Lambda$ case the opposite trend is obtained. Indeed, as explicitly pointed out in [12], no bound ΞN states are expected in the ESC04 parameter set. On the other hand, the FSS model calculations [13] exhibit a completely different energy behavior of the phase-shifts for the same $I = 0$ ΞN channel. The phase shift values are smaller and, in particular, are carrying positive signs indicating an attractive ΞN-interaction.

Note that both models lead also to different predictions for the single-particle (s.p.) in-medium potential of Λ and, in particular, of the cascade particles. As discussed in detail in Refs. [9, 27] in the framework of G-matrix calculations, the in-medium s.p. Λ-potential is in both cases attractive with values between -38 MeV and -45 MeV in the ESC and FFS models, respectively, for matter at saturation density following roughly the quark-scaling rule of a reduction by a factor of 2/3 with respect to the NN-case. The in-medium cascade potentials are rather uncertain, ranging at saturation density from repulsion (ESC) to weak attraction (FFS). In order to keep the present discussion transparent, we will use for the s.p. mean-field potentials the same quark-counting scheme for both models.

The question arises whether such different model predictions for the $S = -2$ YN-interaction can be constrained experimentally by P̄ANDA. In spite of the pronounced model dependencies, an answer on this question is not trivial, because of secondary processes. Indeed, in contrast to free space scattering, in hadron-induced nuclear reactions sequential re-scattering also occurs, for instance, quasi-elastic hyperon–nucleon re-scattering with strangeness exchange ($\Lambda N \leftrightarrow \Sigma N$).

For this purpose we use the elastic and inelastic cross sections for ΞN-scattering for both models in a newly derived parametrizations. In our approach we are accounting also for a smooth transition into the high-energy regime ($E > 3.4$ GeV for baryon–baryon collisions), where the PYTHIA [28] generator is switched on. The parametrizations used for numerical purpose in the transport calculations, which fit the ESC and FSS calculations very well, have been extracted with piecewise polynomial fits.

3. Transport-theoretical approach to multi-strangeness production

For the theoretical description of the antiproton-induced primary reactions and the subsequently generated secondary reac-
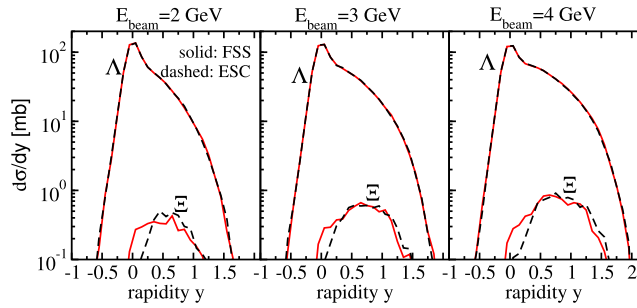
Fig. 2. Rapidity distributions of Λ and Ξ hyperons, as indicated, for $\bar{p}$-induced reactions on Cu-target at $\bar{p}$-beam energies of 2, 3 and 4 GeV for the panel on the left, middle and right, respectively. Transport calculations with the ΞN-parametrizations according to the ESC [12] (dashed curves) and to the FSS [13] (solid curves) models are shown.

tions with a Ξ-beam we adopt the well-established relativistic Boltzmann–Uheling–Uhlenbeck (BUU) transport approach [29]. The kinetic equations are numerically realized within the Giessen–BUU (GiBUU) transport model [30], where the transport equation is given by

$$\left[k^{*\mu}\partial_\mu^x + \left(k_\nu^* F^{\mu\nu} + m^*\partial_x^\mu m^*\right)\partial_\mu^{k^*}\right]f\left(x, k^*\right) = \mathcal{I}_{coll}. \tag{1}$$

Eq. (1) describes the dynamical evolution of the one-body phase-space distribution function $f(x, k^*)$ for the hadrons under the influence of a hadronic mean-field (l.h.s. of Eq. (1)) and binary collisions (r.h.s. of Eq. (1)). The mean-field is treated within the relativistic mean-field approximation of Quantum Hadro-Dynamics [31]. It enters into the transport equation through the kinetic 4-momenta $k^{*\mu} = k^\mu - \Sigma^\mu$ and effective (Dirac) masses $m^* = M - \Sigma_s$. The in-medium self-energies, $\Sigma^\mu = g_\omega\omega^\mu + \tau_3 g_\rho\rho_3^\mu$ and $\Sigma_s = g_\sigma\sigma$, describe the in-medium interaction of nucleons ($\tau_3 = \pm 1$ for protons and neutrons, respectively). The isoscalar, scalar σ, the isoscalar, vector ω^μ and the third isospin-component of the isovector, vector meson field ρ_3^μ are obtained from the standard Lagrangian equations of motion [31]. The obvious parameters (meson–nucleon couplings) are taken from the widely used parametrizations including non-linear self-interactions of the σ field [32]. The meson–hyperon couplings at the mean-field level are obtained from the nucleonic sector using simply quark-counting arguments. The collision term includes all necessary binary processes for (anti)baryon–(anti)baryon, meson–baryon and meson–meson scattering and annihilation [30]. Important for the present work is the implementation of the new parametrizations for the ΞN-scattering processes, as discussed in the previous section. Having the cross sections for all relevant exclusive elementary channels, the collision integral of the transport equation is then modeled with standard Monte Carlo techniques.

4. Strangeness production in $\bar{p}$-induced reactions

We have performed transport calculations for $\bar{p}$-induced reactions including the secondary collisions of Ξ-beams and on a second target. We focus our studies on the role of the ΞN-interaction models on the reaction dynamics and start the discussion with the primary $\bar{p}$-induced reactions.

Fig. 2 show the rapidity spectra of Λ and Ξ hyperons at $\bar{p}$-beam energies of 2, 3 and 4 GeV on a Cu target. At first, the $S = -1$ hyperon distributions are not affected by the choice of the ΞN model. This is due to the fact that the Λ hyperons are mainly produced by $\bar{p}p$ primary annihilation and, in particular, get re-distributed by many secondary processes involving sequential re-scattering of antikaons ($\bar{K}$) and hyperonic $S = -1$ resonances.
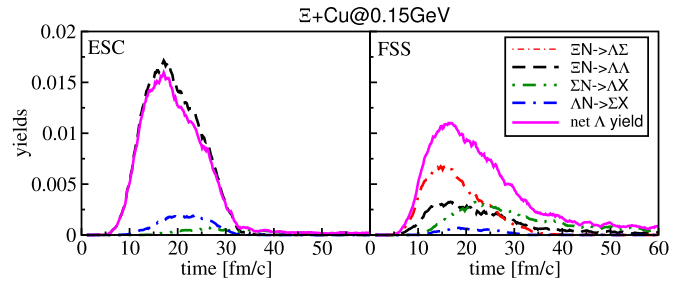

Fig. 3. Time evolution of the net Λ yields (solid curves) and of the contributions of the exclusive channels $\Xi N \rightarrow \Lambda\Lambda$ (dashed curves), $\Xi N \rightarrow \Lambda\Sigma$ (dot-dashed curves), $\Sigma N \rightarrow \Lambda X$ (dot-dot-dashed curves) and $\Lambda N \rightarrow \Sigma X$ (dot-dashed-dashed curves), where X stands for everything else. The yields are normalized to the number of events. Transport calculations using the ESC (left panel) and FSS (right panel) parametrizations are shown for central ($b = 0$ fm) Ξ-induced reaction on Cu-target at a beam Ξ-energy of 0.15 GeV.

The secondary processes in the $S = -1$ sector make the Λ distributions broad and unaffected by the particular treatment of the ΞN interaction. Hence, Λ production will serve to explore independently the $S = -1$ sector.

The production of Ξ particles is a comparatively rare process, as clearly seen in Fig. 2 by the strong decrease of the Ξ-rapidity distributions. This is due to the small values of the direct annihilation cross section $\bar{p}p \rightarrow \bar{\Xi}\Xi$, which is in the range of a few micro-barns only [33]. Note that the corresponding annihilation cross section into $\bar{\Lambda}\Lambda$ pairs is in the range of a few hundreds of micro-barn [33]. As in the case of Λ particles, re-scattering contributes also to the broadness of the Ξ rapidity spectra. However, the effect is less pronounced here due to the high production threshold of the Ξ particles. They mainly escape from the residual excited target nucleus.

The Ξ-yields are rather stable and only moderately dependent on the choice of the ΞN-interaction model. The results with the FSS ΞN-cross sections (solid curves in Fig. 2) lead to increased re-scattering and thus to a shift of the Ξ-spectra to lower energies, relative to the transport calculations using the ESC ΞN-cross sections (dashed curves in Fig. 2). This is obvious by looking at the high-energy part of the elastic cross sections in Fig. 1, where σ_{el} strongly decreases with increasing Ξ-energy, in particular, in the ESC calculations.

5. Multi-strangeness production in Ξ-induced reactions

In $\overline{P}$ANDA the low-energy part of the cascade particles is expected to be used in a second step as a secondary beam. They will react with a secondary target and may produce double-strangeness hypernuclei thus giving access to $S = -2$ hypermatter [22]. Since the underlying theoretical models for the ΞN-interaction exhibit the largest differences at low energies, it is of great interest to study in detail the role of the different ΞN-approaches to the dynamics of Ξ-induced reactions. In order to investigate such processes in this section, we consider the ΞN-reactions as "primary" reactions, although under realistic experimental conditions the Ξ hyperons are produced in an initial annihilation process.

Fig. 3 shows the time evolution of the net Λ yield (solid curves) together with the corresponding contributions to Λ production/absorption, for Ξ-induced reactions on a Cu-target. At first, both sets of transport calculations result to a similar total net Λ yield. The calculations using ESC (FSS) parametrizations lead to values of 0.242 (0.243), respectively, for the total net Λ relative yield (normalized to the number of GiBUU events).

However, the reaction dynamics strongly depend on the underlying approach for the ΞN-interaction. The transport calculations adopting the ESC model (panel on the left in Fig. 3) lead to less

dynamical effects and less re-scattering processes between the Ξ-beam and the target nucleons. In fact, the primary $\Xi N \to \Lambda\Lambda$ binary process mainly dominates the dynamics and contributes basically to Λ hyperon production. These findings are compatible with the ESC-based results in Fig. 1, where the inelastic $\Xi N \to \Lambda\Lambda$ elementary channel strongly dominates among the elastic channels. Note that the $\Xi N \to \Lambda\Sigma$ elementary process does not appear at all. In particular, the $\Xi N \to \Lambda\Sigma$ cross section in the ESC model is very small as compared to the $\Xi N \to \Lambda\Lambda$ channel and in the order of a few mb only. Therefore, secondary $\Sigma N \to \Lambda N$ re-scattering only moderately affect the dynamics of the Ξ–nucleus reaction.

The situation is different in the transport calculations using the FSS approach (panel on the right in Fig. 3). In contrast to the results in the ESC model, the $\Xi N \to \Lambda\Lambda$ primary process is not the dominant one. Indeed, as one can see in Fig. 3, also the primary $\Xi N \to \Lambda\Sigma$ channel occurs. It gives the major contribution to Λ production. This result is also consistent with Fig. 6 of Ref. [13], where at this energy ($E_\Xi = 0.15$ GeV kinetic energy in the laboratory respectively $P_{lab} = 0.646$ GeV/c) the Σ production channel opens. This enhances the Σ production and thus the secondary processes with strangeness exchange, e.g., $\Sigma N \to \Lambda N$. This feature together with the additional issue that elastic and inelastic channels in the FSS approach are of the same order, enhances the dynamical effects of the Ξ particles inside the target nucleus such that the relaxation time of Λ production increases.

6. Formation of multi-strangeness hypernuclei

We thus conclude that the underlying ΞN-interaction has important dynamical effects in low-energy Ξ-induced reactions thus expecting essential observable signals in the formation of $S = -2$ hypernuclei. This underlines the large physics potential of future $S = -2$ production experiments at P̄ANDA. For this reason we study now the formation of double-strangeness hypernuclei in Ξ-induced reactions and the impact of the ΞN-interaction on the hypernuclear yields.

The identification of hypernuclei in the transport calculations is performed as in detail reported in previous work [34]. At first, one applies the statistical multifragmentation model (SMM) [35] to the freeze-out configuration of the residual nucleus. This method provide us with stable and cold fragments (SMM-fragments). As a next step, a momentum coalescence between those SMM-fragments and hyperons is performed leading to capture and providing us finally with hyperfragments.

For the formation of hypernuclei the momentum spectra of hyperons are crucial. It is therefore of great interest to study the model dependencies of the ΞN-interaction on the momentum distributions of strangeness production. Fig. 4 shows this in terms of the rapidity distributions of Λ (panels on the left) and Ξ particles (panels on the right) for Ξ-induced reactions at three low energies, as indicated. At first, the stopping power of Λ hyperons increases in the calculations with the FSS interaction compared to the ESC model. This is because of the enhanced re-scattering involving Λ particles by the FSS interaction. Again, the total Λ yields do not essentially depend on the underlying ΞN-interaction model, but the detailed dynamics does.

The rapidity distributions of the cascade hyperons (panels on the right in Fig. 4) turn out to be more interesting. The calculations with the FSS parametrizations give clear evidence on the appearance of bound Ξ-hyperons inside the target nucleus (thick solid curves in Fig. 4), while in the results using the ESC model the probability of having bound cascade matter is extremely low (thick dashed curves in Fig. 4). In our calculations we identify bound particles as those particles whose radial distance is less than the target ground state radius plus 2 fm. Note that these
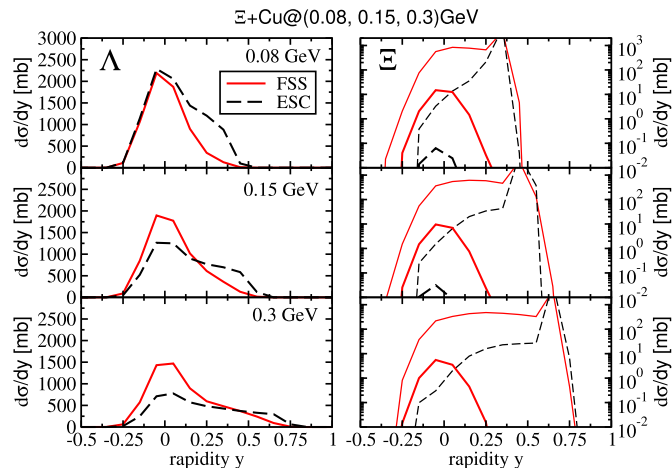

Fig. 4. Rapidity distributions for Λ (panels on the left) and Ξ (panels on the right) particles for Ξ-induced reaction on Cu-target. Transport calculations using the ESC (dashed curves) and FSS (solid curves) parametrizations at three Ξ-beam energies (as indicated) are shown. The additional thick dashed (thick solid) curves on the right panels indicate the rapidity distributions of bound Ξ particles only using the ESC (FSS) parametrizations.

spectra are extracted at the final stage of the reaction, e.g., at 60 fm/c. Thus, particles which are still inside the nucleus at large time scales (relative to freeze-out) can be definitely considered as bound particles. At capture, the Ξ particles carry an average velocity $\bar{\beta}_\Xi = \langle v/c \rangle \sim 0.11$ which is much smaller than e.g. the average velocity of a nucleon at the Fermi-surface, $\bar{\beta}_N \sim 0.25$. The coalescence volume in phase space is thus defined by R and $\bar{\beta}_\Xi$.

This new feature, reported here for the first time, is indeed very promising for the formation of multi-strangeness hypermatter at P̄ANDA (see below). The occurrence of bound cascade hyperons is attributed to the small inelastic cross sections in the FSS model. In fact, as one can see in Fig. 1 (and also in Fig. 6 of Ref. [13] for $\Xi N \to \Lambda\Sigma$), the inelastic $\Xi N \to \Lambda\Lambda$ cross sections are smaller relative to the elastic ones. Therefore, the secondary Ξ-beam particles can enter deeper into the target matter and get captured by re-scattering and decelerating with target constituents. On the other hand, the probability of having bound Ξ hyperons in the ESC-based transport calculations is obviously extremely low.

We have analyzed these transport calculations at different Ξ-beam Energies in terms of (hyper)fragmentation. At first, we have found that the mass distributions become broader around the target mass region and the fission region around half the initial target mass number A_{init} is getting filled with matter as the Ξ-beam energy increases. This is a typical feature of statistical thermodynamical models like the SMM, where with increasing beam energy the excitation of the residual nucleus increases and thus more fragmentation processes (fission, de-excitation) open as the available energy increases.

Such an example of fragment distributions is shown in Fig. 5 for SMM-fragments, double-Λ clusters and Ξ-hypernuclei versus their mass number for inclusive Ξ-induced reactions at a beam energy of 0.3 GeV. It can be seen that both distributions of SMM fragments and double-Λ clusters become moderately broader in the transport calculations using the FSS parametrizations (panel on the right in Fig. 5) as compared to the results using the ESC model (panel on the left in Fig. 5). This is due to the increased re-scattering processes inside the target nucleus in the FSS-based calculations, as discussed in the previous section. This leads to more internal excitation of the residual nucleus and thus to a more pronounced fragmentation dynamics leading to increased fragment yields.
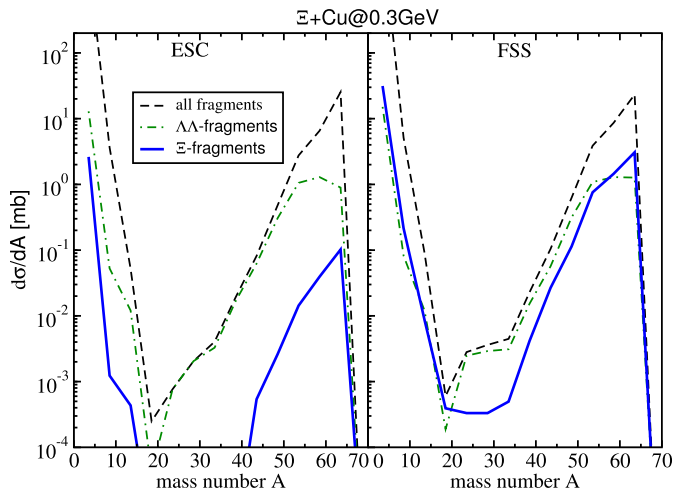
Fig. 5. Mass distributions of pure fragments (dashed curves), double-Λ fragments (dot-dashed curves) and Ξ hyperfragments (thick solid curves). Two sets of calculations are shown, namely one using the ESC (panel on the left) and another one using the FSS models (panel on the right). The considered reactions are inclusive Ξ-induced reactions at a beam Ξ-energy of 0.3 GeV (respectively 0.937 GeV/c beam Ξ-momentum).

The most interesting feature in Fig. 5 is the strong dependence of the distributions of Ξ-bound hypernuclei on the underlying ΞN model. While in the dynamical calculations with the ESC model the production probability of bound Ξ-matter is relatively low, the calculations using the FSS interactions enhances the production of multi-strange Ξ-systems considerably. Another result of great interest is the prediction of Ξ-hypernuclei also far away from the regions of ordinary nuclei, e.g., evaporation ($A \sim A_{init}$) and multifragmentation ($A \leq 4$). This can be clearly seen in Fig. 5, where the fission region ($A \sim A_{init}/2$) is filled up by Ξ-hypermatter in the calculations with the FSS model. This region remains free of multi-strangeness Ξ-hypersystems in the ESC-based transport calculations.

The differences are of such a magnitude that a sizeable spread is predicted for the $S = -2$ production cross sections. It would be therefore a challenge to measure exotic multi-strangeness hypermatter at $\overline{P}$ANDA in the future, in order to better constrain the experimentally still unknown and theoretically very controversial ΞN-interaction, eventually ruling out certain approaches to YN and YY interactions.

7. Summary and conclusions

In summary, we have extended our previous studies on hypernuclear physics by the consideration of more recent models for the high strangeness $S = -2$ sector and their possible influences on observables in reactions relevant for FAIR. For this purpose we have studied first the differences between two well-established models for the ΞN-interaction and then parametrized their results. Applications of ΞN-interaction models in the dynamics of hadron-induced reactions are discussed in detail for the first time.

We found important dynamical effects for reactions at $\overline{P}$ANDA, depending essentially on the underlying ΞN-approach. Strong inelastic (absorption) effects in the elementary scattering channels lead to less dynamical effects in Ξ-induced reactions, while in the opposite case of less pronounced inelasticity the in-medium dynamics is enhanced. As a consequence, bound cascade particles occur in hadron-induced reactions in the case of an attractive ΞN-interaction model.

A coalescence analysis is performed to study the production of (multi-)strangeness hypernuclei in low energy Ξ-induced reactions

using two models for the ΞN-interaction. It is found that the distributions of pure fragments and double-Λ hyperclusters depend only moderately on the applied ΞN-model. However, the role of the ΞN-interaction is found to be essential in the formation of multi-strangeness Ξ-hypernuclei. In fact, models which predict an attractive ΞN interaction on a microscopic level, lead also to a copious production of Ξ-bound hypermatter at $\overline{P}$ANDA, while in the opposite case the formation of such multi-strangeness systems is a rare process. In particular, we predict the formation of possible exotic multi-strangeness hypermatter in Ξ-induced reactions. However, there are still remaining uncertainties on the Ξ mean-field dynamics, which we have not studied separately. We consider the investigations presented here as pilot studies serving to constrain the production of $S = -2$ hypernuclei.

We thus conclude the challenge of the future activities at FAIR to understand deeper the still little known high strangeness sector of the hadronic equation of state. Note that the strangeness sector of the baryonic equation of state is crucial for our knowledge in nuclear and hadron physics and astrophysics. For instance, hyperons in nuclei do not experience Pauli blocking within the Fermi-sea of nucleons. Thus they are well suited for explorations of single-particle dynamics. In highly compressed matter in neutron stars the formation of particles with strangeness degree of freedom is energetically allowed. Of particular interest are hereby the Λ-, Σ-, Ξ- and Ω-hyperons with strangeness $S = -1, -2$ and -3, respectively. As shown in recent studies [36,37], these hyperons modify the stiffness of the baryonic EoS at high densities considerably leading to the puzzling disagreement with recent observations of neutron stars in the range of 2 solar masses.

References

[1] J. Haidenbauer, U.-G. Meissner, A. Nogga, H. Polinder, Lect. Notes Phys. 724 (2007) 113.
[2] E. Friedmann, A. Gal, Phys. Rep. 452 (2007) 89.
[3] B.F. Gibson, E.V. Hungerford, Phys. Rep. 257 (1995) 349.
[4] A.D. Wroblewski, Acta Phys. Pol. B 35 (2004) 901.
[5] J. Schaffner-Bielich, Nucl. Phys. A 804 (2008) 309, arXiv:0801.3791 [astro-ph].
[6] B. Holzenkamp, K. Holinde, J. Speth, Nucl. Phys. A 500 (1989) 485;
    A. Reuber, K. Holinde, J. Speth, Nucl. Phys. A 570 (1994) 543.
[7] Y. Fujiwara, C. Nakamoto, Y. Suzuki, Phys. Rev. 54 (1996) 2180;
    M. Kohno, et al., Nucl. Phys. A 674 (2000) 229;
    Y. Fujiwara, Y. Suzuki, C. Nakamoto, Prog. Part. Nucl. Phys. 58 (2007) 439.
[8] A. Valcarce, et al., Rep. Prog. Phys. 68 (2005) 965, arXiv:hep-ph/0502173.
[9] Th.A. Rijken, V.G.J. Stoks, Y. Yamamoto, Phys. Rev. 59 (1999) 21;
    Th.A. Rijken, Phys. Rev. C 73 (2006) 044007;
    Th.A. Rijken, Y. Yamamoto, Phys. Rev. C 73 (2006) 044008.
[10] K. Sasaki, E. Oset, M.J. Vicente Vacas, Phys. Rev. C 74 (2006) 064002;
    H. Polinder, J. Haidenbauer, U.-G. Meissner, Phys. Lett. B 653 (2007) 29.
[11] J.K. Ahn, et al., Phys. Lett. B 633 (2006) 214.
[12] Th.A. Rijken, Y. Yamamoto, arXiv:nucl-th/0608074.
[13] Y. Fujiwara, et al., Phys. Rev. C 64 (2001) 054001.
[14] T. Gaitanos, et al., Nucl. Phys. A 914 (2013) 405.
[15] J. Steinheimer, et al., J. Phys. Conf. Ser. 389 (2012) 012022.
[16] A.S. Botvina, et al., Nucl. Phys. A 881 (2012) 228.
[17] A.S. Botvina, J. Pochodzalla, Phys. Rev. C 76 (2007) 024909, arXiv:0705.2968 [nucl-th].
[18] A.M. Faessler, et al., Phys. Lett. B 46 (1973) 468;
    R.E. Chrien, et al., Phys. Lett. B 89 (1979) 31;
    M. Akei, et al., Nucl. Phys. A 534 (1991) 478;
    F. Dohrmann, et al., Phys. Rev. Lett. 93 (2004) 242501.
[19] O. Hashimoto, H. Tamura, Prog. Part. Nucl. Phys. 57 (2006) 564.
[20] N. Herrmann, et al., FOPI Collaboration, Hyperfine Interact. 210 (2012) 65.
[21] T.R. Saito, et al., HypHI Collaboration, Nucl. Phys. A 835 (2010) 110.

[22] M.F.M. Lutz, et al., PANDA Collaboration, arXiv:0903.3905 [hep-ex].
[23] A. Esser, et al., Nucl. Phys. A 914 (2013) 519.
[24] A.B. Larionov, T. Gaitanos, U. Mosel, Phys. Rev. C 85 (2012) 024614, arXiv: 1107.2326 [nucl-th].
[25] T. Gaitanos, H. Lenske, U. Mosel, Phys. Lett. B 663 (2008) 197, arXiv:0712.3292 [nucl-th].
[26] T. Gaitanos, H. Lenske, U. Mosel, Phys. Lett. B 675 (2009) 297, arXiv:0904.2106 [nucl-th].
[27] M. Kohno, Y. Fujiwara, Phys. Rev. C 79 (2009) 054318.
[28] T. Sjostrand, S. Mrenna, P.Z. Skands, J. High Energy Phys. 0605 (2006) 026, arXiv:hep-ph/0603175.
[29] W. Botermans, R. Malfliet, Phys. Rep. 198 (1990) 115.
[30] O. Buss, et al., Phys. Rep. 512 (2012) 1, arXiv:1106.1344 [hep-ph].
[31] H.-P. Duerr, Phys. Rev. 103 (1956) 469;
J. Walecka, Ann. Phys. 83 (1974) 491;
B.D. Serot, J.D. Walecka, Int. J. Mod. Phys. E 6 (1997) 515.
[32] G.A. Lalazissis, et al., Phys. Lett. B 671 (2009) 36.
[33] Landolt-Börnstein, New Series I/12b, http://dx.doi.org/10.1007/b35211.
[34] T. Gaitanos, et al., Nucl. Phys. A 881 (2012) 240.
[35] A.S. Botvina, et al., Nucl. Phys. A 475 (1987) 663;
J.P. Bondorf, et al., Phys. Rep. 257 (1995) 133.
[36] J. Schaffner, I.N. Mishustin, Phys. Rev. C 53 (1996) 1416.
[37] S. Weissenborn, D. Chatterjee, J. Schaffner-Bielich, Nucl. Phys. A 881 (2012) 62, arXiv:1111.6049 [astro-ph.HE].